Korean J. Chem. Eng., 34(3), 651-663 (2017)
DOI: 10.1007/s11814-016-0133-3

pISSN: 0256-1115
eISSN: 1975-7220

CFD study on the radial distribution of coolants in the inlet section of rod-baffle-multi-tubular reactor

Cheng Liu*,, Lei Zhang*,**, Yekun Xu*,**, and Yonghui Li*,**,†**

*Key Laboratory for Green Chemical Technology of the Ministry of Education, Tianjin University R&D Center for Petrochemical Technology, Tianjin 300072, China
**Collaborative Innovation Center of Chemical Science and Engineering, Tianjin 300072, China
(*Received 7 March 2016 • accepted 7 May 2016*)

Abstract−CFD method was employed to investigate the radial distribution of coolants in the inlet section of rod baffle multi-tubular reactor. It was found that the reactor had poor distribution of coolants. In view of this problem, the detailed structures of incident channel, shape of baffle ring and distance between tube plate and the first rod baffle were discussed to study their effect on the radial distribution. The simulation results showed that incident channels $0^{\#}$, $1^{\#}$, $3^{\#}$, $5^{\#}$ and $6^{\#}$ could improve radial distribution of coolants significantly, and the effect of incident channels $2^{\#}$ and $4^{\#}$ was relatively limited. The zigzag baffle ring was proved to prevent short pass near the shell wall. In addition, the radial distribution of coolants was also improved with distance between tube plate and the first rod baffle increasing from 85 mm to 242 mm. The simulation results can provide guidance for designing multi-tubular reactor with rod baffles.

Keywords: CFD, Rod Baffle Multi-tubular Reactor, Flow Distribution, Incident Channel

INTRODUCTION

The multi-tubular fixed bed reactor is widely used in the strong exothermic reactions, because of its operational flexibility, simple manufacture and high reliability [1]. In Fig. 1(a) multi-tubular reactor (MTR) uses plate baffle to enhance heat transfer process and support tube bundle. This is the most widely used type in the chemical industry. In the shell side, cross flow is dominant accompanied by vibration of tube bundles [2], high pressure drop and large dead zone in the back of baffles. To solve the above problems, Phillips Petroleum Co. proposed the concept of rod baffle heat exchanger in 1970s [3,4].

Rod baffle consists of support rods, baffle ring, partition blockage plates and longitudinal slide bars or draft rods. These support rods are fixed by baffle ring. Fig. 1(b) illustrates the structure of rod baffles [5]. Fig. 1(c) represents structure of a set of rod baffles [6]. In one rod baffle, all support rods are in parallel. The rods in two adjacent baffles are perpendicular, and all of support rods are perpendicular to axial direction [7,8]. MTR is very similar to multi-tubular heat exchanger in structure. Therefore, there is a possibility to use the research results of rod baffle multi-tubular heat exchanger for reference to develop rod baffle MTR.

Recently, considerable research has been conducted on structure improvement of rod baffle multi-tubular heat exchanger. Wang et al. [9] used a threaded tube instead of a smooth one in the rod baffle heat exchanger. Under the same operating condition, heat-transfer coefficient of the heat exchanger with threaded pipe was up to 300-700 W/(m^2·K), about 38% higher than that of the heat

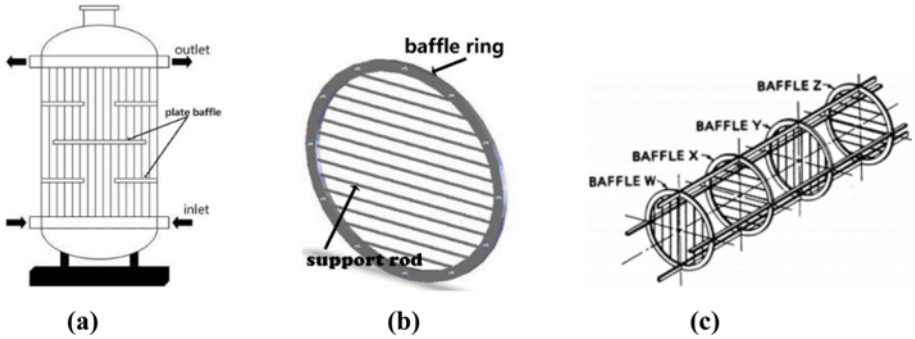

Fig. 1. The structure of Plate baffle MTR (a), Rod baffle (b) and a set of Rod baffles (c).

†To whom correspondence should be addressed.
E-mail: Liyh@tju.edu.cn

exchanger with smooth tube. However, pressure drops of both were nearly equal. Yan et al. [10,11] used wavelike rod instead of straight rod to support tube bundles in the triangular arrangement. Total heat-transfer coefficient varied from 1,000 W/(m^2·K) to 1,300 W/(m^2·K) when Reynolds number was changed from 1.5×10^4 to 5.5×10^4, which was better than that of the corresponding rod baffle heat exchanger. Dong et al. [12] adopted CFD software and the periodic flow unit duct model to simulate shell side of rod baffle heat exchanger. Compared with conclusions obtained by Phillips Petroleum Co., the deviation of heat transfer coefficient and pressure drop was within 10% and 15%, respectively. Wu et al. [13] used periodic total cross-section model to simulate a rod baffle heat exchanger. Compared with the same sized baffle heat exchanger, the rod baffle heat exchanger has the advantage of flow uniformity and small dead zone. Guo et al. [14] used segmented solid model to investigate the effect of inlet, outlet and draft tube on rod baffle heat exchanger. It was found that only at the high Reynolds number can the draft tube enhance the performance of the rod baffle heat exchanger.

However, the rod baffle multi-tubular reactor requires a good radial distribution of coolants in the shell side. This is different from the heat exchanger which only requires the heat load. Furthermore, the diameter of rod baffle MTR is usually much larger than that of the heat exchanger. The uniform distribution of coolants in the shell side becomes very important to the reactor. Most researches have focused on the rod baffle multi-tubular heat exchanger instead of the flow distribution in the shell side of rod baffle MTR. In addition, in the shell side of the reactor the axial flow is predominant, which means that a uniform distribution of coolants in the shell side of the whole reactor is achieved when the distribution in the inlet section is uniform. Therefore, this paper mainly studied the flow distribution in the inlet section to improve the performance of the reactor.

MODELING DETAILS

1. Geometrical Model and Mesh Generation

As seen in Fig. 1(a), the structure of rod baffle MTR was of symmetry. So one-fourth of the reactor was selected as a model, which is sketched as Fig. 2(a). The geometrical specifications of model are given in Table 1. In the simulation, a double supported rod baffle in the Fig. 2(b) was adopted, mainly because cross flow existed in the inlet section and reaction tubes need strong support.

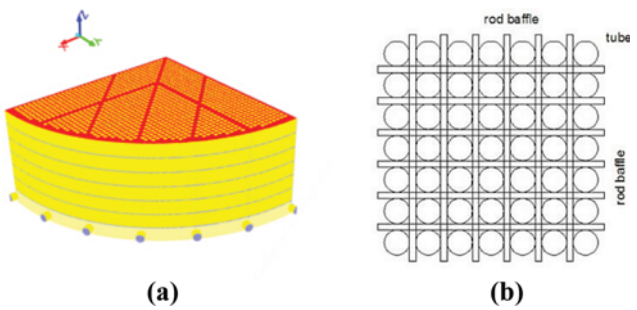

Fig. 2. The structure of the inlet section model (a) and double supported rod baffle (b).

Table 1. The geometrical parameters of model

Structure parameters	Values/mm
Shell radius	1975
Model length	1042
Tube outer diameter	38
Tube pitch	48
Tube bundle geometry	Square
Tube bundle radius	1925
Baffle ring inner radius	1928
Baffle ring outer radius	1972
Support rod shape	Square
Support rod arrangement	Bidirectional support
Support rod width	8
Rod baffle pitch	150
Inlet arrangement	Every other 15°
Inlet diameter	85
Distance from inlet center to tube plate	71
Distance from inlet center to the first rod baffle	71

To simplify the model, the structure was simplified as follows.

(1) Based on research of Bai et al. [15], 24 outlets of distributor were seen as 24 inlets of rod baffle MTR which have the same flux;

(2) Ignore influence of longitudinal slide bars, expansion joint and draft rods of rod baffle;

(3) Ignore detailed structures between support rods and reaction tubes.

The block mesh-generation method was adopted to generate a structured mesh. In each region a face mesh was generated, and volume mesh was created by Cooper method. The initial face mesh size of the inlet region and axial size was 6 mm. In rod baffle region face the mesh size and axial size were 1.33 mm and 2.67 mm, respectively. In the no rod baffle region, face mesh size and axial size were 3.3 mm and 12 mm, respectively. The mesh-generation method could ensure that three nodes existed among the adjacent walls at least. For a model with different configurations, the number of the mesh was about 2.1×10^7. There is not a mesh with negative volume, and the maximum equiangular skew of mesh was below 0.7.

2. Mathematical Model

According to inlet section model, a mathematical model was established as follows. The numerical simulation was performed with a three-dimensional, steady-state and turbulent flow system. The segregated solver and standard k-ε model were employed and energy equation was included. Second-order upwind scheme was chosen to discretize the momentum equation and energy equation. Standard scheme was adopted to discretize pressure. SIMPLEC algorithm was used for pressure-velocity coupling.

In the simulation, the following conditions were set up: work liquid was water; inlet velocity was 4 m/s; the bulk temperature was 438.15 K; the wall heat flux was 1,000 W/m^2; the boundary condition of outlet was outflow. No slip condition was assigned to all walls.

3. Governing Equation

In the simulation, physical properties of water, for example, density, viscosity and specific heat, were constant. Flow was fully tur-

bulent and incompressible. The effect of molecular viscosity was neglected. No net mass addition and other user-defined source term were included. Based on the assumptions, mass, momentum and energy conservation equations were written as follows.

Conservation of mass:

$$\frac{\partial u}{\partial x}+\frac{\partial v}{\partial y}+\frac{\partial w}{\partial z}=0 \tag{1}$$

X-momentum:

$$\rho\left(u\frac{\partial u}{\partial x}+v\frac{\partial u}{\partial y}+w\frac{\partial u}{\partial z}\right)=-\frac{\partial p}{\partial x}+\mu\left(\frac{\partial^2 u}{\partial x^2}+\frac{\partial^2 u}{\partial y^2}+\frac{\partial^2 u}{\partial z^2}\right) \tag{2}$$

Y-momentum:

$$\rho\left(u\frac{\partial v}{\partial x}+v\frac{\partial v}{\partial y}+w\frac{\partial v}{\partial z}\right)=-\frac{\partial p}{\partial y}+\mu\left(\frac{\partial^2 v}{\partial x^2}+\frac{\partial^2 v}{\partial y^2}+\frac{\partial^2 v}{\partial^2 z}\right) \tag{3}$$

Z-momentum:

$$\rho\left(u\frac{\partial w}{\partial x}+v\frac{\partial w}{\partial y}+w\frac{\partial w}{\partial z}\right)=-\frac{\partial p}{\partial z}+\mu\left(\frac{\partial^2 w}{\partial x^2}+\frac{\partial^2 w}{\partial y^2}+\frac{\partial^2 w}{\partial z^2}\right) \tag{4}$$

Conservation of energy:

$$\rho C_p\left(u\frac{\partial T}{\partial x}+v\frac{\partial T}{\partial y}+w\frac{\partial T}{\partial z}\right)=\lambda\left(\frac{\partial^2 T}{\partial x^2}+\frac{\partial^2 T}{\partial y^2}+\frac{\partial^2 T}{\partial z^2}\right) \tag{5}$$

The turbulence kinetic energy, κ, and the dissipation rate, ε, were obtained from the following equations [16].

$$\rho\frac{\partial \kappa}{\partial t}+\rho\frac{\partial(\kappa u_i)}{\partial x_i}=\frac{\partial}{\partial x_i}\left[\left(\mu+\frac{\mu_t}{\sigma_\kappa}\right)\frac{\partial \kappa}{\partial x_j}\right]+G_\kappa-\rho\varepsilon \tag{6}$$

$$\rho\frac{\partial \varepsilon}{\partial t}+\rho\frac{\partial(\varepsilon u_i)}{\partial x_i}=\frac{\partial}{\partial x_j}\left[\left(\mu+\frac{\mu_t}{\sigma_\varepsilon}\right)\frac{\partial \varepsilon}{\partial x_j}\right]+G_\kappa\frac{C_{1\varepsilon}\varepsilon}{\kappa}-C_{2\varepsilon}\rho\frac{\varepsilon 2}{\kappa} \tag{7}$$

In Eqs. (6) and (7), G_κ represents generation of turbulence kinetic energy due to mean velocity gradients. $C_{1\varepsilon}$ and $C_{2\varepsilon}$ are empirical constants. σ_κ and σ_ε are turbulent Prandtl numbers for k and ε, respectively. The constant values were 1.44, 1.92, 1.0 and 1.3 for $C_{1\varepsilon}$, $C_{2\varepsilon}$, σ_κ and σ_ε, respectively.

In Eq. (8), wall heat transfer film coefficient, H_w [16], was defined to measure uniformity of radial distribution.

$$H_w=\frac{\rho C_p C_\mu^{0.5}\kappa_p^{0.25}}{T^*} \tag{8}$$

$$T^*=\begin{cases} Pry^* & y^*<y_T^* \\ Pr_t\left[\frac{1}{\kappa}\ln(Ey^*)+P\right] & y^*>y_T^* \end{cases} \tag{9}$$

In Eq. (9) [16], y_T^* represents distance from mesh nodes in the first layer to wall. κ is Von Karman constant, 0.4187. E is also constant, 9.737. P was calculated as follows.

$$P=9.24\left[\left(\frac{Pr}{Pr_t}\right)^{3/4}-1\right]\left(1+0.28e^{-\frac{0.007Pr}{Pr_t}}\right) \tag{10}$$

In Eq. (10) [16], Pr represents molecular Prandtl number. Pr_t is turbulent Prandtl number.

MODEL VALIDATION AND FLOW DISTRIBUTION

To validate the reliability of the mathematical model, the simulation results were compared with the results from engineering correlations and experimental investigations.

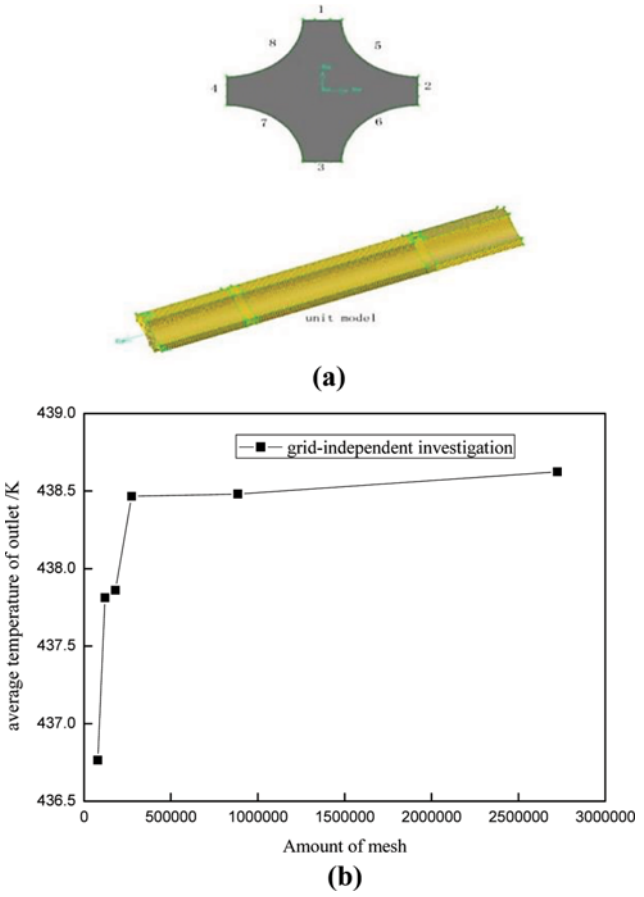

Fig. 3. Geometric model of unit model (a) and grid-independent investigation (b).

1. Heat Transfer Validation

In the simulation, the unit model in the Fig. 3(a) was used to investigate the heat transfer. In the model, faces 1-4 were set as symmetry conditions, and faces 5-8 were set as heat-wall face conditions. The two end faces of the model were set as velocity-inlet condition and pressure-outlet condition, respectively. The grid-independent solution was obtained in Fig. 3(b). Finally, 885188 mixed cells were included in the model.

In the heat transfer validation for reliability of numerical simulation, Eq. (11) and (12), two kinds of practical engineering correlations of heat transfer coefficient [17,18], were used.

$$Nu=0.0859Re^{0.815}\cdot Pr^{1/3}\cdot\left(\frac{L_b}{d_e}\right)^{-0.303}\cdot\left(\frac{\mu}{\mu_w}\right)^{0.14} \tag{11}$$

$$Nu=C_T Re^{0.8}\cdot Pr^{0.4}\cdot\left(\frac{\mu}{\mu_w}\right)^{0.14} \tag{12}$$

where L_b is baffle spacing, and d_e in Eq. (13) is the equivalent diameter of unit model. C_T is the turbulent heat transfer geometry coefficient, which is determined by the geometry condition of rod baffle heat exchanger. Re is the Reynolds number of fluid on the shell side, which is defined by Eq. (14).

Table 2. Heat transfer coefficient from numerical simulation and engineering correlations (L_b=150 mm)

U (m/s)	0.05	0.06	0.07	0.08	0.095	0.10
t_i (K)	420.15	420.15	420.15	420.15	420.15	420.15
t_o (K)	438.48	435.22	432.89	431.15	429.26	428.76
h (W/(m^2·K))	1241.96	1406.04	1563.07	1716.17	1944.25	2019.84
h_t (W/(m^2·K))	1302.51	1509.93	1707.02	1899.06	2179.16	2270.78
Error (%)	4.65	6.88	8.43	9.63	10.78	11.05
h_p (W/(m^2·K))	1106.65	1279.67	1444.19	1604.14	1836.88	1912.87
Error (%)	−12.23	−9.88	−8.23	−6.98	−5.84	−5.59

h_t- calculated by Eq. (11), h_P-calculated by Eq. (12)

$$d_e = \frac{4(P_T^2 - \pi d_o^2/4)}{\pi d_o} \tag{13}$$

$$Re = \frac{\rho u d_e}{\mu} \tag{14}$$

where u represents fluid velocity on the shell side. P_T is the tube pitch size and d_o is the tube outside diameter.

The heat transfer coefficient comparison between numerical simulations and engineering correlations at different inlet velocities is listed in Table 2.

In Table 2, the heat transfer coefficient errors between simulation results and practical engineering correlations were within 15%. Therefore, the mathematical model and unit model were receivable to compute the heat transfer coefficient.

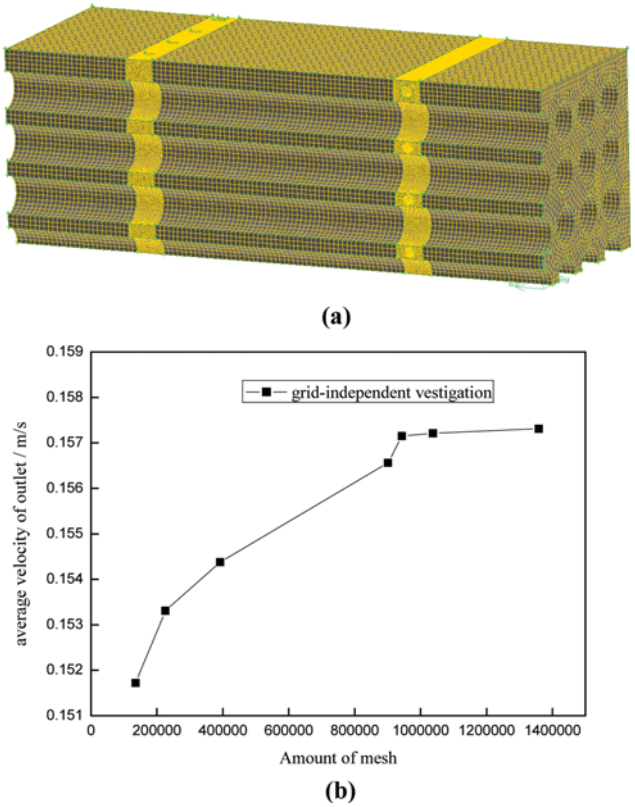

Fig. 4. The structure of numerical model (a) and grid-independent investigation (b).

2. Fluid Flow Validation

To validate the flow field in the shell side of the rod baffle heat exchanger in the simulation, the experiment by Dong et al. [5] was used as benchmark. In the simulation, the one-fourth of the experimental model was built in Gambit, which is described in Fig. 4(a). The grid-independent result was obtained in Fig. 4(b), and the refined model included 903036 mixed cells.

The flow field comparison between the numerical simulation and the experimental results is listed in Table 3.

It is seen in Table 3 that z value is two orders of magnitude higher than y value since the z-direction flow was dominant in the shell side of the rod baffle heat exchanger. Although the errors were larger in y direction between the simulation and the experiment, the z value errors were within 15%. Therefore, it was concluded that the mathematical method could reveal the flow field in the shell side of rod baffle heat exchanger exactly.

3. Flow Distribution in the Shell Side of Rod Baffle MTR

In the simulation, four models were developed to investigate flow distribution in the shell side of rod baffle MTR.

(A) No rod baffle model.

(B) Two rod baffles model where rod baffles are distributed every other 150 mm.

Table 3. Comparison of fluid flow between the numerical simulation and the experimental investigation

Measured point	1	2	3
z (m/s)Experimental value	0.2179	0.2164	0.2053
Numerical value	0.1881	0.1891	0.1914
Error/%	−13.70	−12.61	−6.75
y (m/s)Experimental value	0.0048	0.0045	0.0024
Numerical value	0.0094	0.0009	0.0027
Error/%	94.73	−80.20	11.35
Measured point	7	8	9
z (m/s)Experimental value	0.2040	0.2039	0.2059
Numerical value	0.1874	0.1840	0.1886
Error/%	−8.13	−9.74	−8.38
y(m/s)Experimental value	0.0052	0.0041	0.0036
Numerical value	0.0099	0.0068	−0.0007
Error/%	89.82	64.36	−121.13

z- fluid velocity in positive z direction, y- fluid velocity in negative y direction

(C) Four rod baffles model where rod baffles are distributed every other 150 mm.

(D) Six rod baffles model where rod baffles are distributed every other 150 mm.

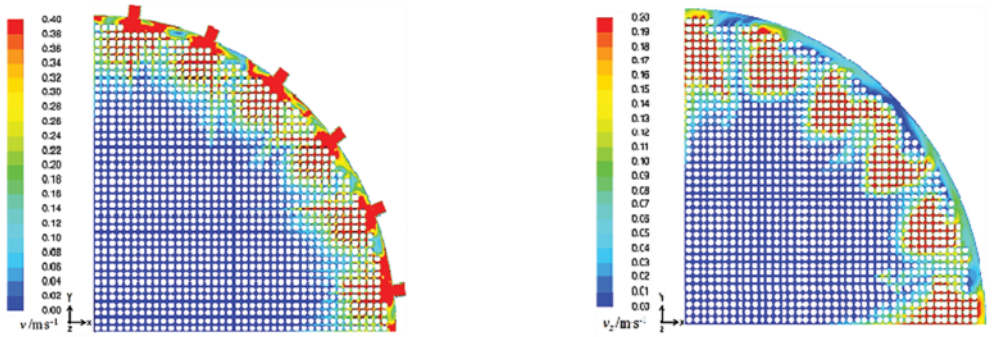

model A

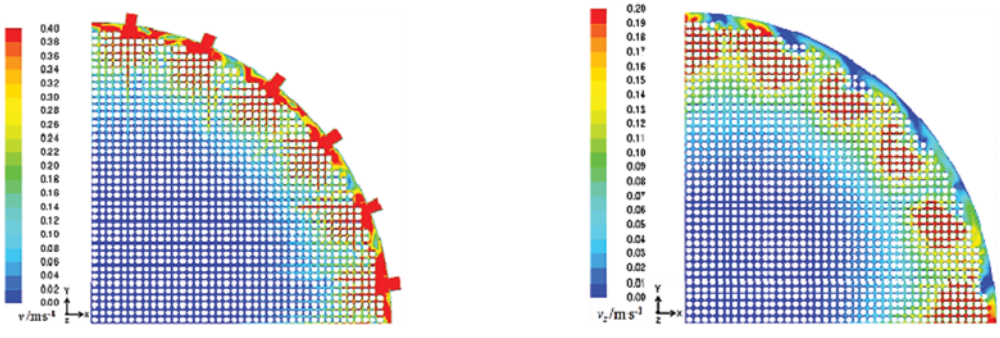

model B

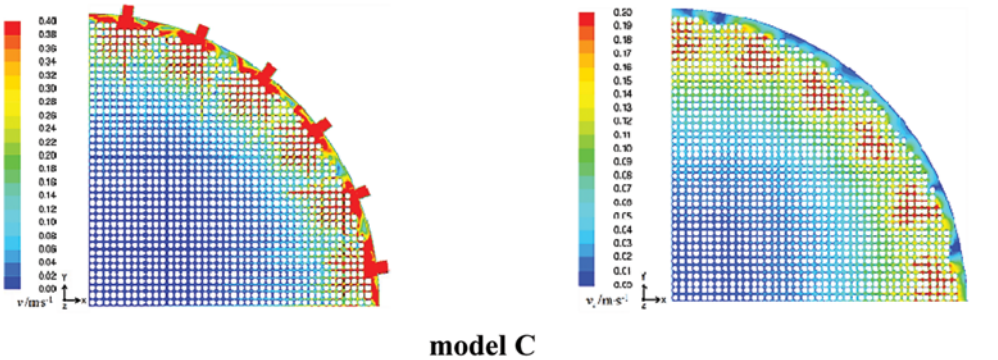

model C

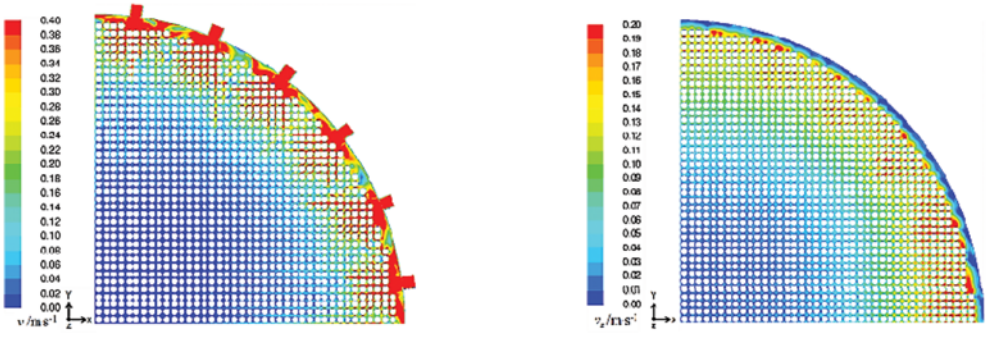

model D

(a)

Fig. 5. Velocity contours of inlet (left), outlet (right) cross section of model A, B, C and D (a) and Velocity contours of longitudinal section of model A, B, C and D (b).

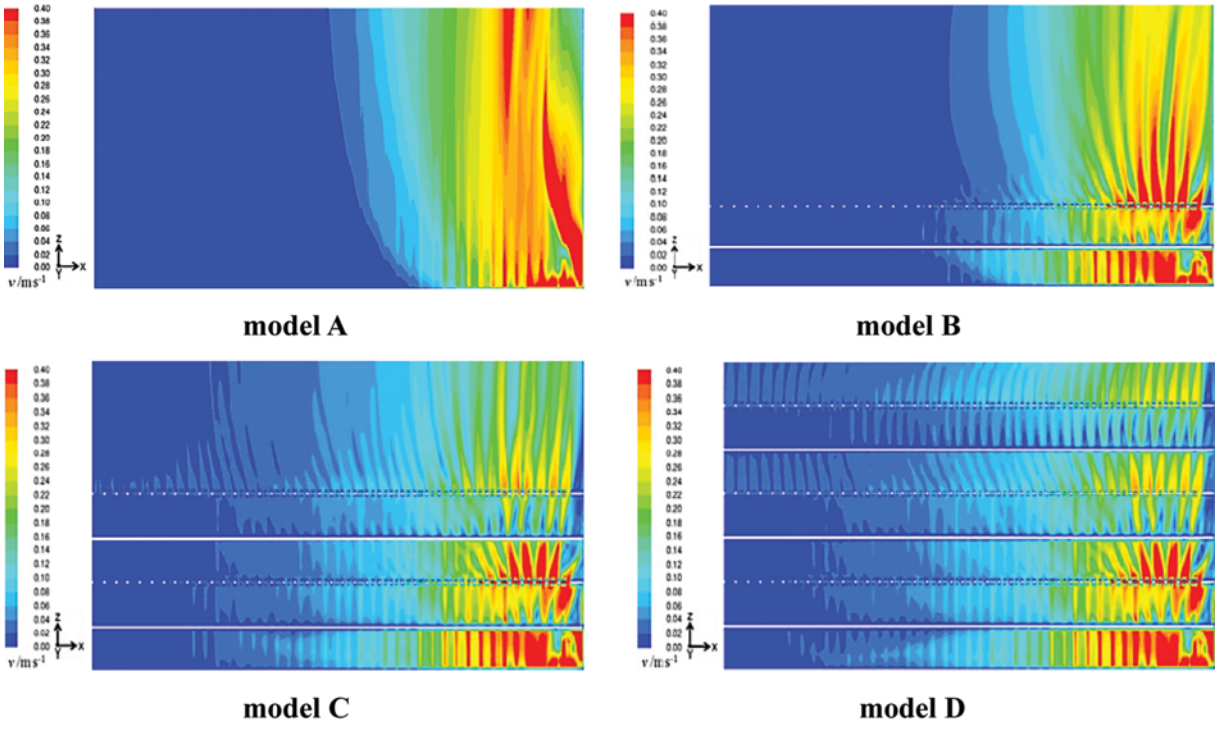

Fig. 5. Continued.

These models had similar structures but different amount of rod baffle. The angles between six inlet tubes and X axis were 7.5°, 22.5°, 37.5°, 52.5°, 67.5° and 82.5°, respectively.

Fig. 5 shows the velocity contours of models A, B, C and D. As illustrated in Fig. 5(a), flow velocity near the shell wall was high, especially in the inlet nozzle region, but a large dead zone existed in the central region of the rod baffle MTR. With the increasing number of rod baffles, fluid flowed into the central region. However, flow rate in the central region was still low, even zero (Fig. 5(b)). Consequently it cannot just depend on increasing the amount of rod baffles to achieve radial uniform distribution.

STRUCTURE OPTIMIZATION

To improve the radial flow distribution in the shell side of the reactor, this chapter discusses the effect of incident channel connecting shell wall region with the central region, shape of baffle ring and relative location of tube plate, the first rod baffle and inlet tube.

1. Effect of Incident Channel

One way to solve the issue above was to create incident channels by taking out some reaction tubes. In the section, the influence of incident channels was investigated. A 7.5° change of inlet nozzles direction was needed to locate the incident channels at 45° direction. Reaction tubes, which are at 0°, 45° and 90° angle, were removed. The number of reaction tubes was 1172. Model E was created in Fig. 6(a).

As illustrated in Fig. 6(b), in terms of velocity distribution of inlet cross section, incident channel could promote fluid to flow into the central region. Compared with model D, velocity distribution in outlet cross section of model E was improved. However, velocity difference between the central region and shell wall region was still remarkable.

2. Effect of Baffle Ring Shape

As shown in Fig. 6(b), there were high velocity zones near the shell wall, which meant that a short pass existed. In models D and E circular baffle ring could result in interspace between baffle ring and reaction tubes. To eliminate the phenomenon, zigzag baffle ring was used instead of the circular one [19]. Therefore, model F based on model E was created in Fig. 7(a).

As seen in Fig. 7(b), the velocity distribution in the inlet cross section of model F changed little, since baffle rings and inlet cross section were not at the same height. However, the high velocity area in the outlet cross section of model F decreased obviously. Therefore, the zigzag baffle ring could prevent the short pass near the shell wall.

3. Effect of Number of Incident Channels

In Effect of Incident Channel section incident channels could improve flow distribution. It was reasonable to study the influence of the number of incident channels on the performance of the reactor. For convenience, inlet tubes and corresponding incident channels were named after 0#, 1#, 2#, 3#, 4#, 5# and 6#. Therefore, two new models based on model F were created in Fig. 8(a).

(1) Model G: Incident channels 1# and 5# were set up in front of inlet tubes 1# and 5#, respectively. They were parallel to X and Y axis, respectively. Their end points were located in the incident channel 3#. In addition, rectangle baffles were used in the incident channels. Model G contained 1116 reaction tubes.

(2) Model H: On the basis of model G the new incident chan-

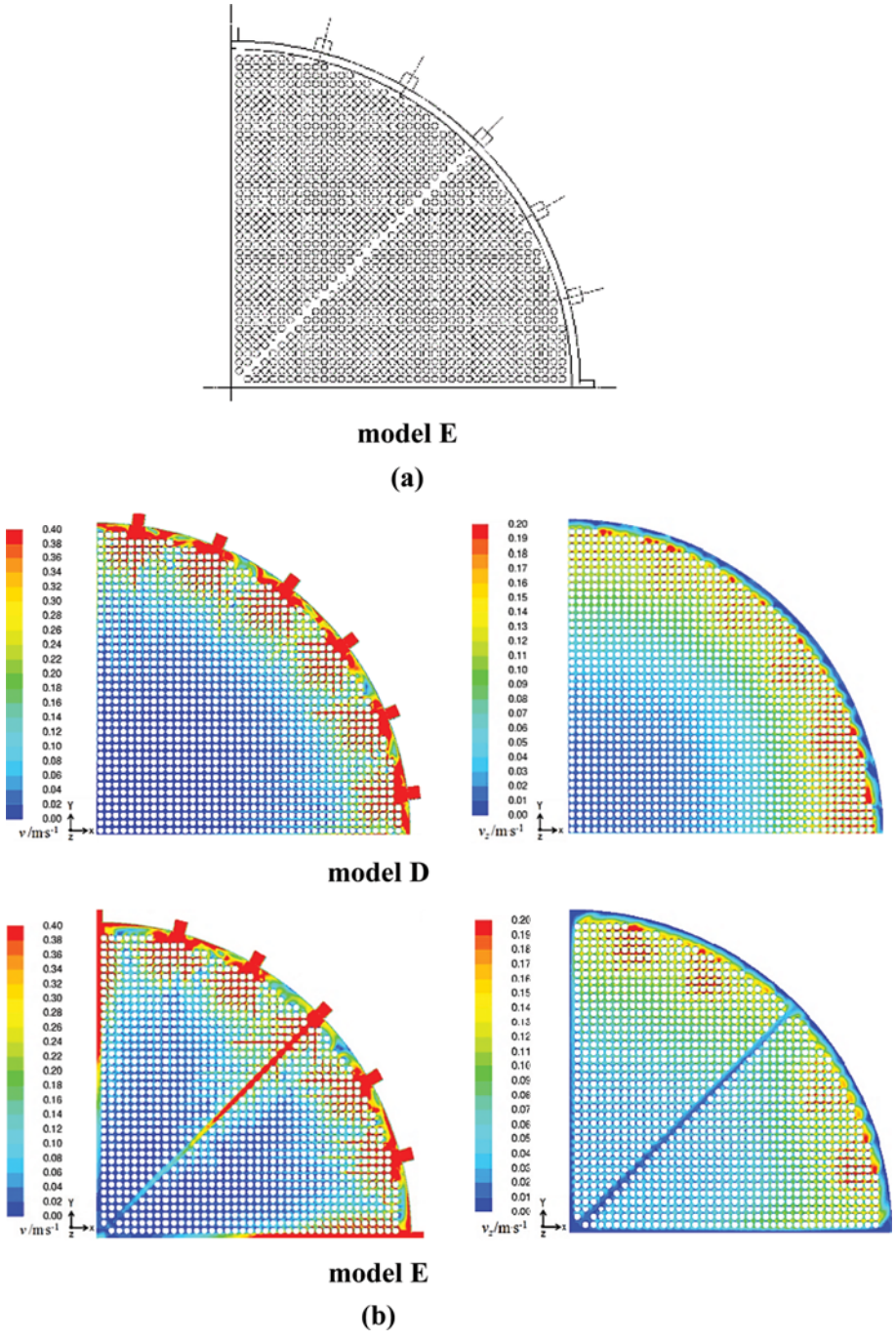

Fig. 6. The structure of model E (a) and Velocity contours of inlet (left), outlet (right) cross section of model D and E (b).

nels $2^{\#}$ and $4^{\#}$ were set up in front of inlet tubes $2^{\#}$ and $4^{\#}$, respectively. The incident channels were parallel to the incident channel $3^{\#}$. Their end points were located in incident channels $1^{\#}$ and $5^{\#}$, respectively. Similarly, rectangle baffles were added in the incident channels. Model H contained 1096 reaction tubes.

In Fig. 8(b) with the number of incident channels increasing, the area of the dead zone gradually decreased. From the velocity distribution of outlet cross section, model H was superior to model F and G, especially in the fan-shaped region.

As described in Fig. 9, the flow distribution of model H was improved further compared with models F and G. It meant incident channels $1^{\#}$, $5^{\#}$ could enhance the uniformity of flow distribution greatly, and incident channels $2^{\#}$ and $4^{\#}$ had limited effect on the performance. Therefore, when the good uniformity of flow distribution was demanded, incident channels $2^{\#}$, $4^{\#}$ should be set up.

4. Effect of Length of the Incident Channel

With the number of incident channels increasing, a dead zone in the central region still existed. It was rational to extend the incident channels. Therefore, in the section models I and J depicted in Fig. 10(a) were created on the basis of models G and H, respec-

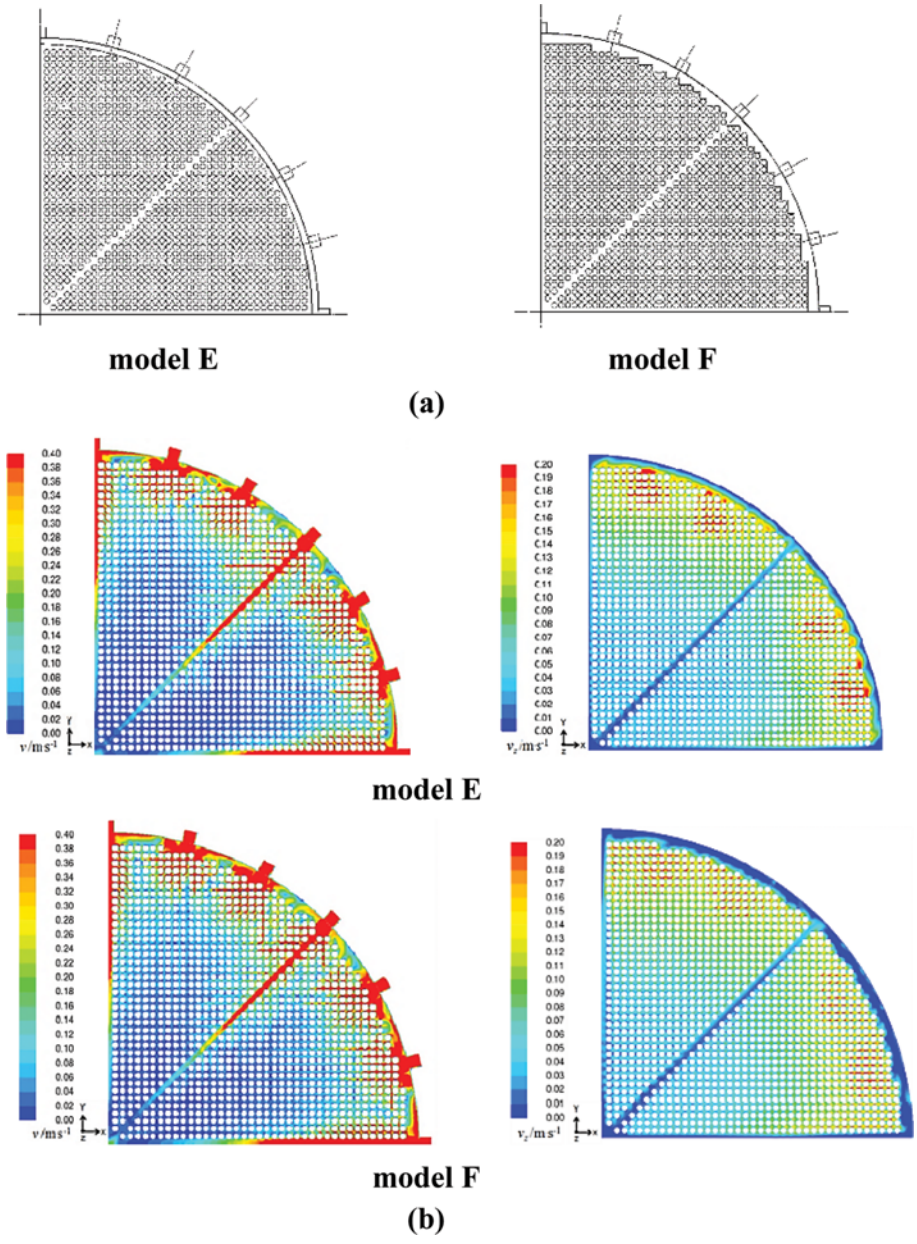

Fig. 7. The structure of model E and F (a) and Velocity contours of inlet (left), outlet (right) cross section of model E and F (b).

tively.

(1) Model I: The incident channels 1# and 5# were stretched to Y and X axis, respectively. The rectangle baffles in incident channels were also extended to X and Y axis. The number of reaction tubes was 1096.

(2) Model J: The incident channels 2# and 4# were extended to X and Y axis, respectively. Likewise, the rectangle baffles in incident channels were also extended to X and Y axis, respectively. The number of reaction tubes was 1078.

As illustrated in Fig. 10(b), in the extended parts of incident channels 1#, 5# flow velocity was still small, while in the extensions of incident channels 2#, 4# flow rate was above 0.22 m/s. Therefore, extensions of incident channels 2#, 4# could enhance the uniformity of the radial flow distribution. From the velocity distribution in the outlet cross section, model J was superior to model I.

In Fig. 11 some conclusions were obtained as follows:

(1) The average heat transfer film coefficient in the central region of models I and J was enhanced because of the extensions of incident channels, but their effect was limited.

(2) In terms of the flow distribution uniformity, model H was superior to model I. So it was concluded that the use of incident channels 2#, 4# was valuable. In reality, the extensions of incident channels 1#, 5# were not adopted.

5. Effect of Distance Among Inlet Tubes, the First Rod Baffle and Tube Plate

In this section, models K and L based on model J were created in Fig. 12(a) to investigate the influence of distance among inlet tubes, the first rod baffle and tube plate on the performance of

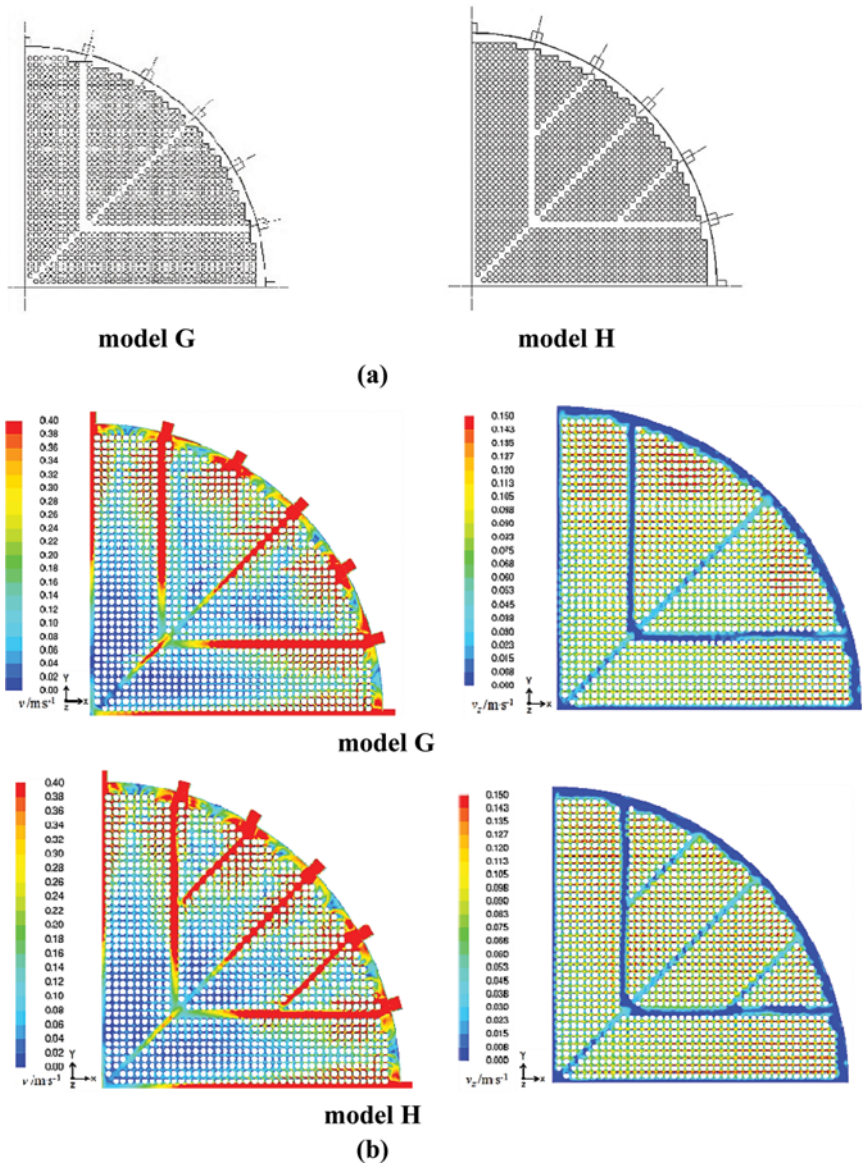

Fig. 8. The structure of model G and H (a) and Velocity contours of inlet (left), outlet (right) cross section of model G and H (b).

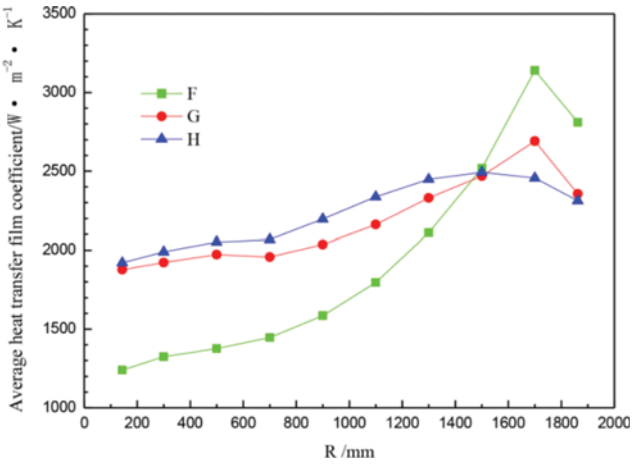

Fig. 9. Average heat transfer film coefficient of model F, G and H vs radius.

reactor.

(1) Model K: The distance between the first rod baffle and tube plate fell to 85 mm. The inlet tube was tangent to the first rod baffle and tube plate.

(2) Model L: With distance between the first rod baffle and tube plate constant, the distance between the inlet tubes and the tube plate fell by 85 mm so the inlet tube was tangent to the tube plate.

From velocity contours of inlet cross section in Fig. 12(b), fluid could be transferred into the central region in model K. In the inlet cross section, the dead zone area of model K was the smallest. However, from velocity distribution of the outlet cross section, the performance of model J was the best.

As shown in Fig. 12(c), the heat transfer distribution of model J was the best. This could be attributed to the relative location of inlet tube, the first rod baffle and tube plate. When fluid was transferred along radial direction, it also flowed along the axial direc-

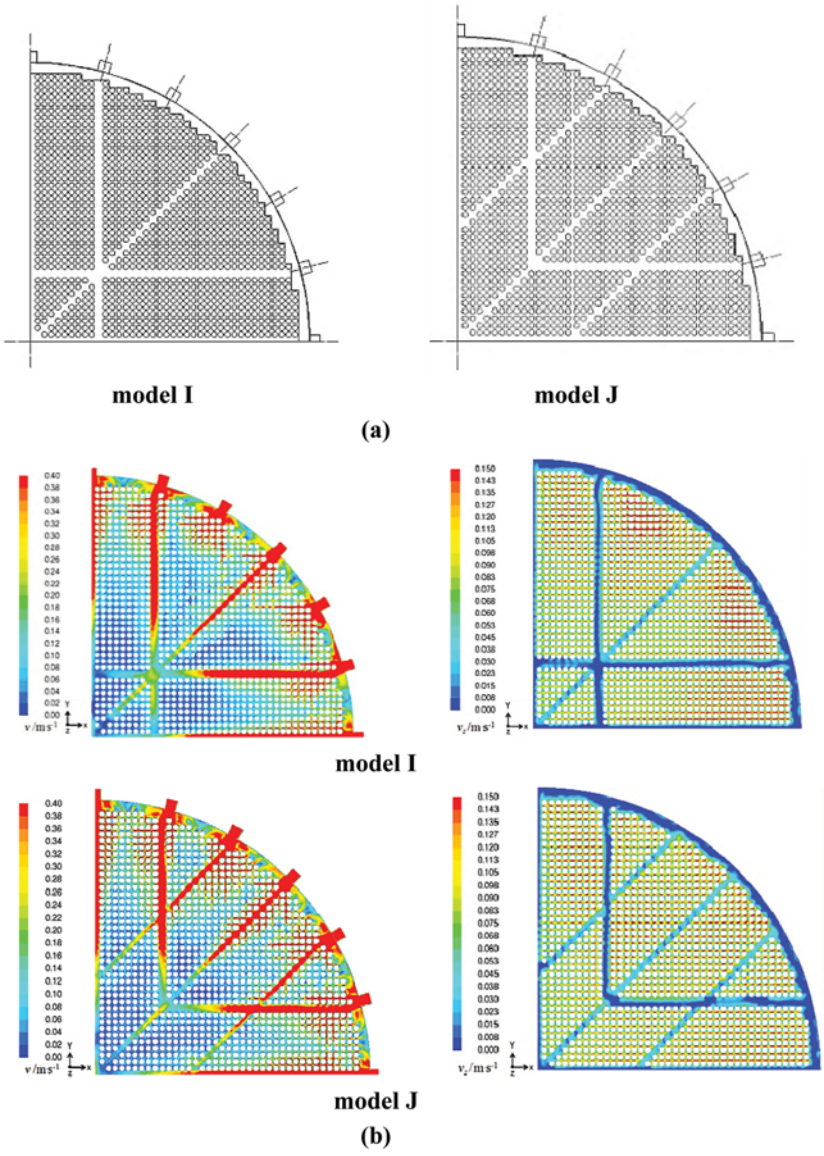

Fig. 10. The structure of models I and J (a) and velocity contours of inlet (left), outlet (right) cross section of model I and J (b).

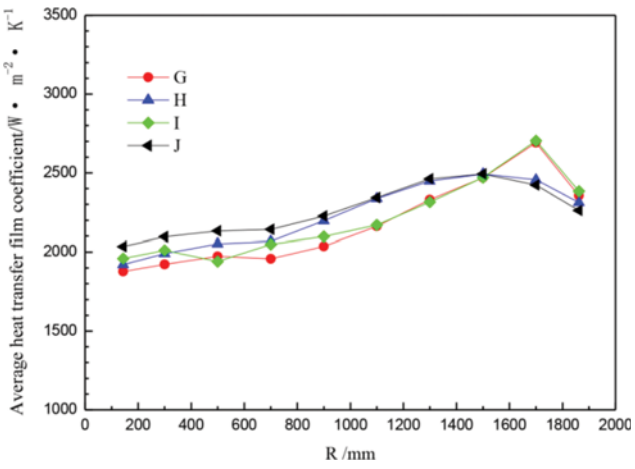

Fig. 11. Average heat transfer film coefficient of model G, H, I and J vs radius.

tion. Therefore, the distance between the first rod baffle and tube plate could determine the flow time, which affected cross flow distance.

Based on the analysis above, the conclusion was obtained that increase of distance among the first rod baffle, inlet tubes and tube plate had a positive influence on the performance of the reactor. In reality, the inlet tubes were generally located in the center of tube plate and the first rod baffle. Thus, the distance between the first rod baffle and tube plate should be investigated further. Models M and N based on model J were created in Fig. 13(a):

(1) Model M: Distance between the first rod baffle and tube plate was increased from 142 mm to 192 mm.

(2) Model N: Distance between the first rod baffle and tube plate was increased from 142 mm to 242 mm.

In Fig. 13(b) it was known that the flow distribution of model N was the best, successively followed by model M, model J and model K. Therefore, it was concluded that increasing the distance between the first rod baffle and tube plate could improve radial

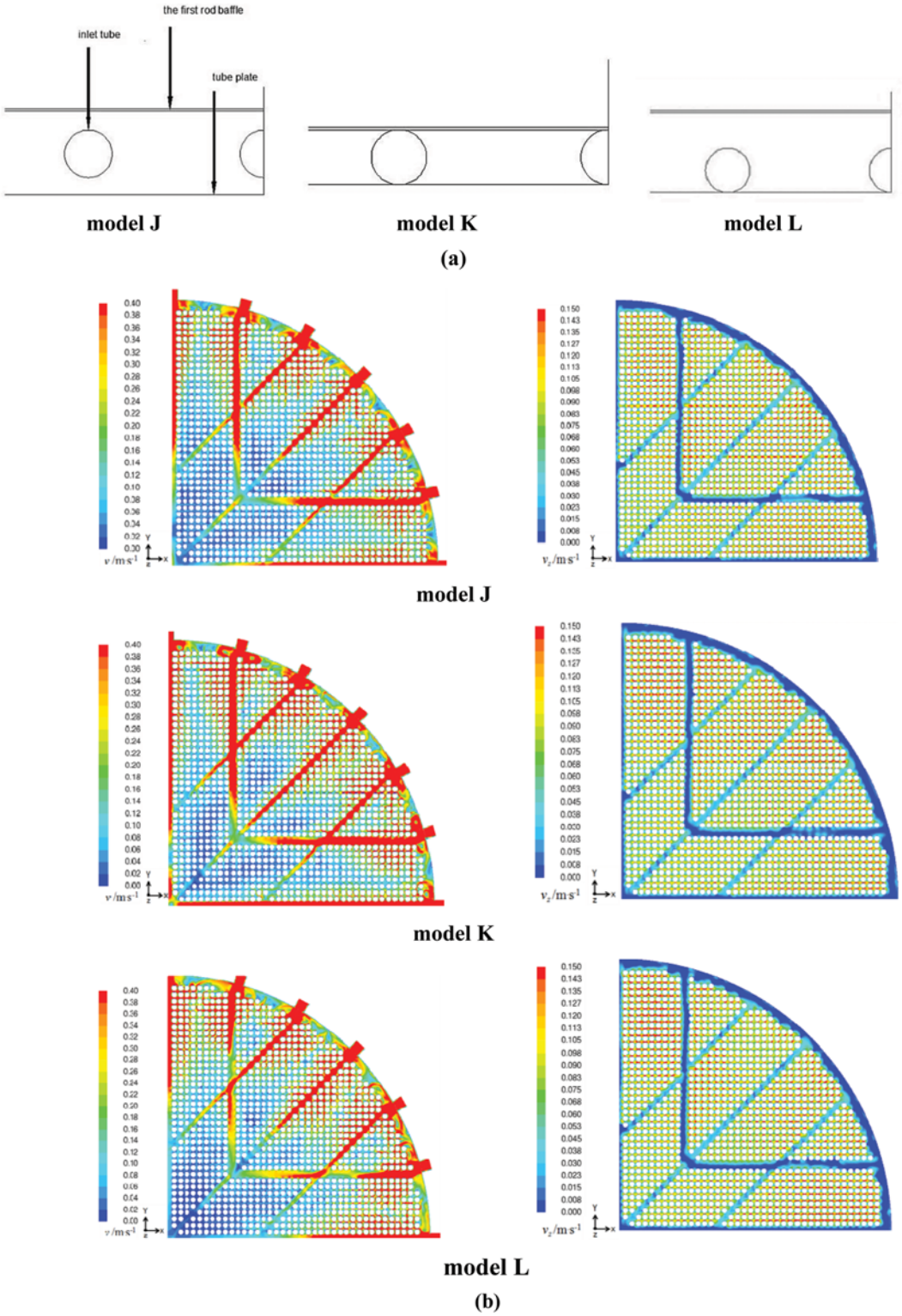

Fig. 12. The structure of models J, K and L (a), velocity contours of inlet (left), outlet (right) cross section of models J, K and L (b) and average heat transfer film coefficient of models J, K and L vs radius (c).

flow distribution, especially when the distance ranged from 85 mm to 242 mm. On the other hand, the distance could not be too big, because reaction tubes need strong support if there is cross flow in the inlet section.

CONCLUSION

CFD method was employed to investigate the radial distribution of coolant, the uniform distribution of which is very import-

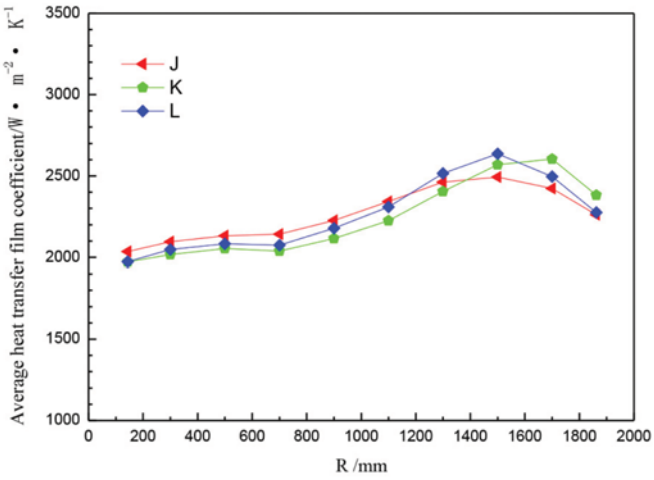

(c)

Fig. 12. Continued.

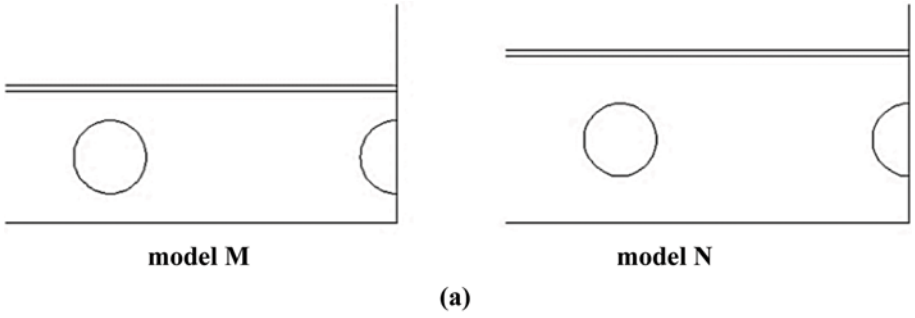

(a)

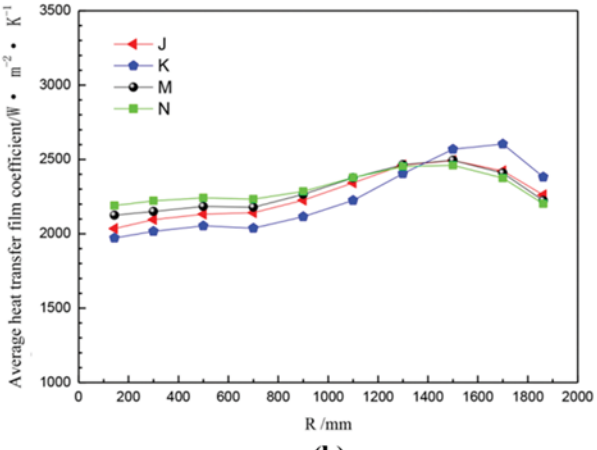

(b)

Fig. 13. The structure of models M and N (a) and average heat transfer film coefficient of models J, K, M and N vs radius (b).

ant for MTR to work efficiently, in the inlet section of MTR with rod baffles. The calculated results indicated that it had poor radial distribution, such as short pass near the shell wall region and flow dead zones in the central region. Some explorations were carried out to improve the distribution of coolant in the inlet section. It was found that the incident channel could promote the coolants to flow into the central region of the reactor and the zigzag baffle ring could prevent the short pass near the shell wall. Furthermore, the detailed structures of the incident channels were optimized. The effect of the number and length of incident channels on the radial distribution of coolants was investigated in the paper. The simulation results showed that incident channels $0^{\#}$, $1^{\#}$, $3^{\#}$, $5^{\#}$ and $6^{\#}$ could improve radial distribution of coolants significantly. Incident channels $2^{\#}$, $4^{\#}$ and their extensions also ameliorated the distribution, but their effect was relatively limited. In addition, the influence of distance between tube plate and the first rod baffle in the inlet section on the radial distribution of coolants was also investigated. The calculated results showed that radial distribution

of coolants was improved with the distance increasing from 85 mm to 242 mm. The simulation results can provide guidance for designing the MTR with rod baffles.

NOMENCLATURE

C_P : specific heat [J·kg^{-1}·K^{-1}]
C_t : turbulent heat transfer geometry coefficient (=0.0589)
C_μ : constant in turbulent model
d_e : equivalent diameter of unit model [m]
G_k : generation of turbulent kinetic energy due to velocity gradient [m^2·s^{-2}]
H_w : wall heat transfer coefficient [W·m^{-2}·K^{-1}]
h_{te} : heat transfer coefficient calculated by TEERC [W·m^{-2}·K^{-1}]
h_p : heat transfer coefficient calculated by Phillips Petroleum Co. [W·m^{-2}·K^{-1}]
Pr : molecular prandtl number
Pr_t : turbulent prandtl number
T : temperature [K]
T^* : dimensionless temperature
y_T^* : distance from nodes in the first layer to wall [m]

Greek Symbols

ρ : density [kg·m^{-3}]
κ : turbulence kinetic energy [m^2·s^{-2}]
ε : turbulence dissipation rate [m^2·s^{-3}]
λ : thermal conductivity [W·m^{-1}·K^{-1}]
μ : dynamic viscosity of fluid [Pa·s]

Subscripts

k : turbulent kinetic
p : Phillips Petroleum Co.
t : turbulence
te : thermal energy engineering research center
w : wall

REFERENCES

1. G. D. Wang, *PetroChem. Equip. Technol.*, **33**(1), 10 (2012).
2. J. E. Eilers and W. M. Small, *Chem. Eng. Prog.*, **69**(7), 57 (1973).
3. W. M. Small and R. K. Young, *Oil Gas J.*, **75**(37), 77 (1977).
4. Y. B. Lin, H. L. Yu and S. J. Yang, *J. Shanghai Univ. Sci. Technol.*, **35**(6), 596 (2013).
5. Q. W. Dong, Y. Q. Wang and M. S. Liu, *Appl. Therm. Eng.*, **28**(7), 651 (2008).
6. B. I. Master, K. S. Chunangad and A. J. Boxma, *Heat Transfer. Eng.*, **27**(6), 4 (2006).
7. L. Y. Kang, *Sci. Technol. Commun.*, **21**(6), 132 (2012).
8. W. Huang, *Chem. Equip. Technol.*, **17**(1), 21 (1999).
9. X. S. Wang, R. Z. Wang and J. Y. Wu, *Appl. Therm. Eng.*, **25**(11-12), 1753 (2005).
10. L. W. Yan, J. X. Wu and Z. W. Wang, *J. Shanghai Univ.: English Edition*, **8**(3), 337 (2004).
11. L. W. Yan and Z. W. Wang, *J. East Chin Univ. Sci. Technol.*, **30**(8), 478 (2004).
12. J. X. Wu, Q. W. Dong and S. M. Liu, *Chem. Ind. Eng. Prog.*, **21**(5), 306, 337 (2002).
13. Y. Wu. *The simulation of inner flow field in the multi-tubular fixed bed reactor [D]*, Tianjin University (2010).
14. C. Z. Guo and C. J. Hu, *Technol. Eng.*, **43**(1), 51 (2013).
15. M. H. Zhang, L. Bai, Z. F. Geng and Y. H. Li, *Chem. Ind. Eng.*, **29**(1), 43 (2012).
16. ANSYS Fluent Theory Guide (2013).
17. Q. W. Dong and M. S. Liu, *Chemical Industry Press*, Beijing (2007).
18. C. C. Gentry, *Chem. Eng. Prog.*, **86**, 48 (1990).
19. C. Zhu and Y. D. Xu, *Henan Chem. Ind.*, **10**, 27 (1998).